Analytica Chimica Acta 1058 (2019) 155–165

Contents lists available at ScienceDirect

Analytica Chimica Acta

journal homepage: www.elsevier.com/locate/aca

A novel and simple imidazo[1,2-a]pyridin fluorescent probe for the sensitive and selective imaging of cysteine in living cells and zebrafish

Meiqing Zhu [a, b], Lijun Wang [a, b], Xiaoqin Wu [b], Risong Na [a, *], Yi Wang [a, b, d, **], Qing X. Li [c], Bruce D. Hammock [d]

[a] Collaborative Innovation Center of Henan Grain Crops, National Key Laboratory of Wheat and Maize Crop Science, College of Plant Protection, Henan Agricultural University, Wenhua Road No. 95, Zhengzhou, 450002, China
[b] Key Laboratory of Agri-food Safety of Anhui Province, School of Resources and Environment, Anhui Agricultural University, Hefei, 230036, China
[c] Department of Molecular Bioscience and Bioengineering, University of Hawaii, 1955 East-West Road, Honolulu, HI, 96822, USA
[d] Department of Entomology and UCD Comprehensive Cancer Center, School of Veterinary Medicine, University of California, Davis, CA, 95616, USA

HIGHLIGHTS

- 2-(Imidazo[1,2-a]pyridin-2-yl)phenyl acrylate (**IPPA**) is a novel fluorescent probe.
- **IPPA** can detect Cys over Hcy, GSH and other analytes.
- **IPPA** can selectively detect as low as 0.33 μM of Cys in DMSO/HEPES buffer.
- **IPPA** has been successfully utilized to image living cells and zebrafish.

GRAPHICAL ABSTRACT

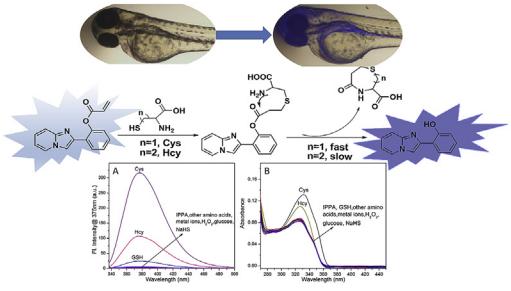

ARTICLE INFO

Article history:
Received 22 October 2018
Received in revised form
27 December 2018
Accepted 21 January 2019
Available online 25 January 2019

Keywords:
Fluorescent probe

ABSTRACT

Cysteine (Cys), homocysteine (Hcy) and glutathione (GSH) play many crucial physiological roles in organisms. Their abnormal levels can cause and indicate various diseases. In the present study, a small-molecule fluorescent probe 2-(imidazo[1,2-a]pyridin-2-yl)phenyl acrylate (**IPPA**) was designed, synthesized and characterized by NMR, FT-IR and HRMS. **IPPA** can selectively detect Cys over other analytes because of an approximately 76 times enhancement in fluorescence intensity. The limit of detection of **IPPA** for Cys was 0.33 μM. The pseudo-first-order rate constant of the reaction between **IPPA** and Cys was approximately 10 times that of the reaction between **IPPA** and Hcy (K_{Cys} 3.18×10^{-3} S^{-1} *vs* K_{Hcy} 4.92×10^{-4} S^{-1}), indicating that Cys can be distinguished from Hcy. In addition, **IPPA** exhibits strong

Abbreviations: Cys, cysteine; Hcy, homocysteine; GSH, glutathione; Pro, proline; Try, tryptophan; Tyr, tyrosine; Arg, arginine; His, histidine; Lys, lysine; Asp, aspartic acid; Thr, threonine; Glu, glutamic acid; Gly, glycine; DFT, density functional theory; DMEM, dulbecco's modified eagle medium; **HPIP**, 2-(imidazo[1,2-a]pyridin-2-yl) phenol; **IPPA**, 2-(imidazo[1,2-a]pyridin-2-yl)phenyl acrylate.

* Corresponding author. Collaborative Innovation Center of Henan Grain Crops, National Key Laboratory of Wheat and Maize Crop Science, College of Plant Protection, Henan Agricultrual University, Wenhua Road No. 95, Zhengzhou, 450002, China

** Corresponding author. Key Laboratory of Agri-food Safety of Anhui Province, School of Resources and Environment, Anhui Agricultural University, Hefei, 230036, China

E-mail addresses: risongna@163.com (R. Na), wangyi1987@cau.edu.cn (Y. Wang).

https://doi.org/10.1016/j.aca.2019.01.023

Cellular detection
Density functional theory calculations
Imaging

anti-interference ability, small molecular weight, high efficiency, low toxicity and good cell permeability. It was successfully used in imaging HepG2 cells and zebrafish. The fluorescence response of **IPPA** for calf serum are powerful proofs for practical application. Therefore, **IPPA** has high potential for bioassay applications.

1. Introduction

Cysteine (Cys), homocysteine (Hcy) and glutathione (GSH) are three biological thiols present in organisms [1–4]. Their metabolism and transport are closely related to the functional expression of many significant enzymes and proteins in the body [5]. Abnormal levels of biothiols in vivo can cause and indicate various diseases. The sulfhydryl group of Cys is an ideal nucleophile in reactions, undergoing a reversible redox reaction under physiological conditions, which is necessary for the formation of disulfide bonds that maintain the tertiary and quaternary structure of proteins [6–9]. Hcy is a key intermediate product derived from Cys by methionine and is closely related to the health of the cardiovascular system [10–12]. GSH participates many cellular activities, such as maintenance of intracellular redox homeostasis, heterogeneous metabolism, intracellular signaling, and gene regulation [9,13,14]. Therefore, quantitative detection of biothiols in organisms can help us understand the role of thiol-containing enzymes or proteins in physiological and pathological processes. It can also provide important information for the prevention and diagnosis of various diseases, theoretically laying the foundation for clinical applications of quantitative biothiol detection methods [15–18].

Traditional methods to detect biothiols include high-performance liquid chromatography [19], mass spectrometry [20], and capillary electrophoresis [19,21]. However, these methods need high-cost equipment, complicated sample processing and long runtime, and are therefore not suitable for high-throughput routine clinical trials and scientific research applications [22–24]. Because of their low detection limit and high selectivity, fluorescent probes have been used for the quantitative detection of biothiols [25–28]. Cho's group [29] reported a two-photon fluorescent probe for the detection of thiols based on a thiol/disulfide exchange. Two-photon microscopy, using two near-infrared photons as the excitation source, has the advantages of a high tissue-penetration depth, localized excitation, and prolonged observation time, thereby allowing tissue imaging. Pang et al. [30] reported a ratiometric biothiol fluorescent probe with an acryloyl group as a recognition site, which can selectively recognize Cys in cells and can be applied to bioluminescence imaging. Kim's group [31,32] developed a chromene molecule that can be used to detect thiol content in solid tumors. The probe exhibits high selectivity, high sensitivity and a ratiometric response in which its yellow fluorescence emission (550 nm) changes to blue fluorescence emission (496 nm), which can effectively eliminate interference from background autofluorescence [31,32]. On the basis of tandem conjugate addition and intramolecular cyclization, Yang et al. [33] developed a fluorescent probe for detection of Cys and the probe shows selectivity for Cys over other biothiols. Up to now, some fluorescent probes can selectively monitor Cys [34–36]. However, most of these probes have complicated structures and large molecular weight, which may not enter the cells or organisms easily in the real applications. Therefore, it is meaningful to develop simple fluorescent probes which can recognize Cys over other analytes.

The acryloyl group was first established as a recognition group in 2011 by Strongin's group [37,38]. It is a classic Michael acceptor with a polarized α-β unsaturated moiety, which can react with the mercapto group of biothiols through a Michael addition reaction [39,40]. Due to the different nucleophilicities of the three biothiols, selective identification of biothiols can be achieved via their different addition reaction rates and cyclization cleavage processes [41–43]. To date, it is still a challenge to distinguish three biothiols completely with fluorescent probes [44–46]. Therefore, a new strategy for the design and development of fluorescent probes for selectively detecting Cys is highly desirable. The acrylate group has a strong electron-withdrawing ability and reactivity with biothiols, undergoing the cyclization and cleavage reaction. Thus, the fluorescence would change with the leaving of the electron-withdrawing groups.

Based on the above strategies, a small-molecule fluorescent probe, 2-(imidazo[1,2-a]pyridin-2-yl)phenyl acrylate (**IPPA**), was designed and synthesized, using 2-(imidazo[1,2-a]pyridin-2-yl) phenol (**HPIP**) as the fluorophore and the acryloyl group as the recognition group. **IPPA** can selectively detect Cys over Hcy, GSH and other analytes due to their different nucleophilicities, addition reaction rates and cyclization cleavage processes. In addition, **IPPA** exhibits low cytotoxicity and good cell permeability and was successfully applied to imaging studies of HepG2 cells and zebrafish.

2. Experimental

2.1. Chemicals and instruments

Cys, Hcy and GSH were purchased from Sigma-Aldrich (St. Louis, MO, USA). Proline (Pro), tryptophan (Try), tyrosine (Tyr), arginine (Arg), histidine (His), lysine (Lys), aspartic acid (Asp), threonine (Thr), glutamic acid (Glu), glycine (Gly), KNO_3, $Ca(NO_3)_2{\cdot}4H_2O$, $NaNO_3$, $Cu(NO_3)_2{\cdot}3H_2O$, $Mg(NO_3)_2{\cdot}6H_2O$, $Zn(NO_3)_2{\cdot}6H_2O$, and $Fe(NO_3)_3{\cdot}9H_2O$ were supplied by Sinopharm Chemical Reagent Co., Ltd. (Shanghai, China) and J&K (Beijing, China). All reagents were used without further purification, unless otherwise specified. Aqueous solutions of metal ions were prepared from the corresponding purchased nitrate salt. The deionized water was obtained from a Milli-Q Plus ultrapure water system (Billerica, MA, USA). HepG2 cells were provided by the Provincial Hospital of Anhui in China.

During the experiment, all fluorescence spectra were recorded in a 1-cm quartz cuvette with a volume of 3.0 mL on a Cary Eclipse fluorescence spectrophotometer (Agilent Technologies, Santa Clara, CA, USA) equipped with a xenon lamp. The slit width was at 10 nm. UV–Vis absorption spectra were measured with a UV-1800 spectrophotometer (Shimadzu, Kyoto, Japan). Mass spectra (MS) and HRMS were collected on a UPLC/XevoTQ MS/MS (Waters, Milford, MA, USA) and an Agilent Accurate-Mass-Q-TOF MS 6520 system equipped with an electrospray ionization (ESI) source. ^{1}H NMR (600 MHz) and ^{13}C NMR (150 MHz) spectra were collected on a spectrometer (Agilent Technologies, Santa Clara, CA, USA) using tetramethylsilane (TMS) as an internal standard. The pH values were measured by a model pH-25 digital display pH meter (Shanghai REX Instrument Factory, Shanghai, China). Fluorescence imaging of HepG2 cells and zebrafish was performed on an EVOS FL

Auto inverted fluorescence microscope (Massachusetts, USA) and a Nikon inverted Ti-S epifluorescence microscope (Tokyo, Japan), respectively.

2.2. Synthesis and characterization of ***IPPA***

2-(Imidazo[1,2-a]pyridin-2-yl)phenol (**HPIP**) [47]. 1-(2-Hydroxyphenyl)ethanone (200 mg, 1.47 mmol), pyridin-2-amine (318 mg, 3.38 mmol) and I_2 (448 mg, 1.78 mmol) were mixed in a round-bottom flask. The mixture was stirred at 110 °C for 4 h and then stirred overnight at 70 °C. After the reaction was completed, an excess amount of NaOH (aq, 45%) was added and the reaction mixture was stirred at 100 °C for 1 h. Then the reaction mixture was cooled to room temperature and diluted with 25 mL of CH_2Cl_2. The pH of the reaction solution was made neutral using HCl (aq, 10%). The mixture was extracted with CH_2Cl_2 and washed with deionized water (3 × 10 mL). The organic phase was dried over anhydrous Na_2SO_4 and concentrated under reduced pressure. The product was isolated using a chromatography column (SiO_2, CH_2Cl_2/n-hexane = 3:1), and recrystallized from an ethanol-water system to give an orange-yellow solid (235 mg, 60%). ^{1}H NMR (600 MHz, DMSO-d_6): δ 12.03 (s, 1H), 8.61–8.57 (m, 1H), 8.46 (s, 1H), 7.86–7.85 (dd, J = 7.7, 1.7 Hz, 1H), 7.65–7.63 (dd, J = 9.0, 1.1 Hz, 1H), 7.33–7.30 (m, 1H), 7.18–7.16 (m, 1H), 6.98–6.95 (dd, J = 6.7, 1.2 Hz, 1H), 6.92–6.86 (m, 2H). HRMS (ESI, m/z) calculated for $[C_{13}H_{10}N_2O + H]^+$: 211.0866, found: 211.0866. IR (KBr, cm^{-1}): 3445.69, 3132.31, 3042.06, 1587.13, 1403.44, 1355.23, 1253.99, 1146.47, 1063.47, 1023.53, 915.54, 840.33, 749.21, 660.50.

2-(Imidazo[1,2-a]pyridin-2-yl)phenyl acrylate (**IPPA**).

2-(Imidazo[1,2-a]pyridin-2-yl)phenol (500 mg, 2.4 mmol) was dissolved in anhydrous CH_2Cl_2 (30 mL) and cooled to 0 °C. Then two equivalents of triethylamine were added to the mixture and acryloyl chloride (270 mg, 3.0 mmol) was slowly added dropwise to the solution. Finally, the temperature of the solution was slowly raised to room temperature and stirred overnight. The progress of the reaction was monitored by a thin-layer chromatography silica gel plate (TLC). The solvent was evaporated to dryness when the reaction was finished. The desired product was obtained by purification of the crude material on a silica gel column (V_{Hexane}: $V_{Ethyl\ acetate}$ = 6:1), white solid, 420 mg, yield: 66.2%, solubility: 46.25 μg/mL in water (25 °C). ^{1}H NMR (600 MHz, DMSO-d_6) δ 8.54 (dt, J = 6.8, 1.2 Hz, 1H), 8.26–8.19 (m, 1H), 8.15 (s, 1H), 7.57–7.52 (m, 1H), 7.42–7.34 (m, 2H), 7.23 (m, 2H), 6.87 (td, J = 6.7, 1.1 Hz, 1H), 6.59 (d, J = 1.7 Hz, 2H), 6.20 (dd, J = 6.6, 5.0 Hz, 1H). ^{13}C NMR (151 MHz, DMSO-d_6) δ 164.59, 147.71, 144.52, 139.96, 134.26, 129.38, 128.91, 128.28, 127.48, 127.03, 126.76, 125.74, 123.78, 117.08, 112.73, 111.75. HRMS (ESI, m/z) calculated for $[C_{16}H_{12}N_2O_2 + H]^+$: 265.0972, found: 265.0971. IR (KBr, cm^{-1}): 3442.83, 3152.68, 3074.06, 1740.18, 1633.80, 1499.35, 1405.49, 1368.19, 1276.49, 1244.21, 1152.40, 1072.95, 1007.07, 902.81, 836.05, 755.37, 741.84, 674.33.

2.3. Fluorescence quantum yield

The fluorescence quantum yield of **IPPA** was calculated by comparison with a quinine sulfate standard solution containing 0.1 M H_2SO_4. The formula for calculating the fluorescence quantum yield is as follows [48–50]:

$$\phi_X = \phi_s(F_X/F_S)(A_S/A_X)\left(\eta_X^2/\eta_S^2\right) \quad (1)$$

where Φ represents the fluorescence quantum yield, and F and A indicate the area of the fluorescent peak after correction and the absorbance at the maximum excitation wavelength, respectively. η is the refractive index of the solvent used, and "s" and "x" represent data for the quinine sulfate standards and calculated samples, respectively.

2.4. Fluorescence and UV–Vis spectra

The measuring conditions of all fluorescence spectra during the experiments were as follows: E_x = 330 nm, slit width of 10 nm, and emission wavelength range of 300–500 nm. The measurement conditions of the UV–Vis spectrum were as follows: the scanning wavelength range is 200–500 nm, and the scanning step is 1.0 nm. **IPPA** stock solution (100 μM) was prepared by dissolving **IPPA** in DMSO solution, and amino acids, metal ions, H_2O_2, NaHS and glucose solutions were prepared using deionized water. The solutions required in the subsequent experiments were all formulated using the above stock solutions, and probe solution was prepared using 2-[4-(2-hydroxyethyl)-1-piperazinyl] ethanesulfonic acid (HEPES) as the buffer solution.

2.5. Cytotoxicity

First, 96-well plates were seeded with HepG2 cells at a density of 4 × 10^4 cells per well. Then the plates were incubated with **IPPA** at a series of concentrations (10, 20, 30, 40 μM) and cells in wells to which no **IPPA** was added were used as a control group. After 24 h of incubation, the cells were rinsed with PBS three times. Then, a CCK-8 assay was used to analyze cell viability. The absorbance was measured at 450 nm by using a microtiter plate reader (ELx808, BioTek, USA).

2.6. Cell imaging of ***IPPA***

HepG2 cells (liver hepatocellular cells) were cultured and maintained in Dulbecco's modified Eagle's medium (DMEM) supplemented with 10% fetal bovine serum (FBS), 100 μg/mL penicillin, and 100 μg/mL streptomycin and incubated at 37 °C under a humidified atmosphere containing 5% CO_2. A stock solution of the probe **IPPA** having a concentration of 10 mM in DMSO was formulated. The above stock solution of the probe was diluted with cell culture solution to 20 μM for cell culture (DMSO content < 0.2%). Next, the cells were incubated with the probe, N-ethylmaleimide (NEM, is mainly used as a block agent for biothiols) or biothiols in the incubator at 37 °C and then rinsed three times with PBS. Fluorescent images were obtained under a fluorescence microscope after three washes with PBS to remove the probe residue.

2.7. Study of zebrafish in vivo imaging

Zebrafish eggs were incubated in E3 embryo medium (15 mM NaCl, 0.5 mM KCl, 1 mM $MgSO_4$, 1 mM $CaCl_2$, 0.15 mM, KH_2PO_4, 0.05 mM Na_2HPO_4, 0.7 mM $NaHCO_3$, and 10^{-5}% methylene blue at pH 7.5). The incubation rate was accelerated by a 12-h light/12-h dark cycle. After 3 days of incubation, the normal-growing zebrafish were selected for the experiment. Zebrafish were incubated with and without 200 μM NEM in E3 medium for 15 min, washed three times with E3 medium to remove the remaining NEM, and further incubated with 20 μM of **IPPA** (DMSO content < 0.2%) in E3 medium for 30 min (28 °C). After washing three times with E3 medium, the zebrafish were imaged under a fluorescence microscope, and untreated zebrafish were used as blank controls.

3. Results and discussion

3.1. Synthesis of *IPPA*

This work mainly utilizes the strong nucleophilicity of sulfhydryl groups in small-molecule biothiols [51–53]. Considering the Michael addition mechanism [54,55], 2-(imidazo[1,2-a]pyridin-2-yl)phenol is used as the fluorophore, and the acrylate group is selected as the recognition site. The acrylate group is a classic Michael acceptor with a polarized α-β unsaturated moiety, which can react with the mercapto group of the biothiols through the Michael addition reaction. Thus, the biothiol fluorescent probe **IPPA** was designed and synthesized. Due to the different nucleophilicities of the three biothiols, selective identification of biothiols can be achieved via their different addition reaction rates and cyclization cleavage processes [56,57]. **IPPA** may enter cells or living tissues easily because of the low molecular weight. The synthetic pathway of **IPPA** is shown in Scheme 1, and **IPPA** was characterized by ^{1}HNMR, ^{13}CNMR, HRMS and IR (Figs. S1–6).

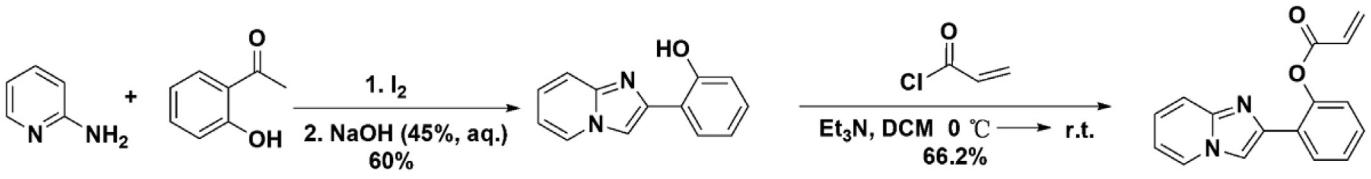

Scheme 1. Synthetic scheme of 2-(imidazo[1,2-a]pyridin-2-yl)phenyl acrylate (**IPPA**).

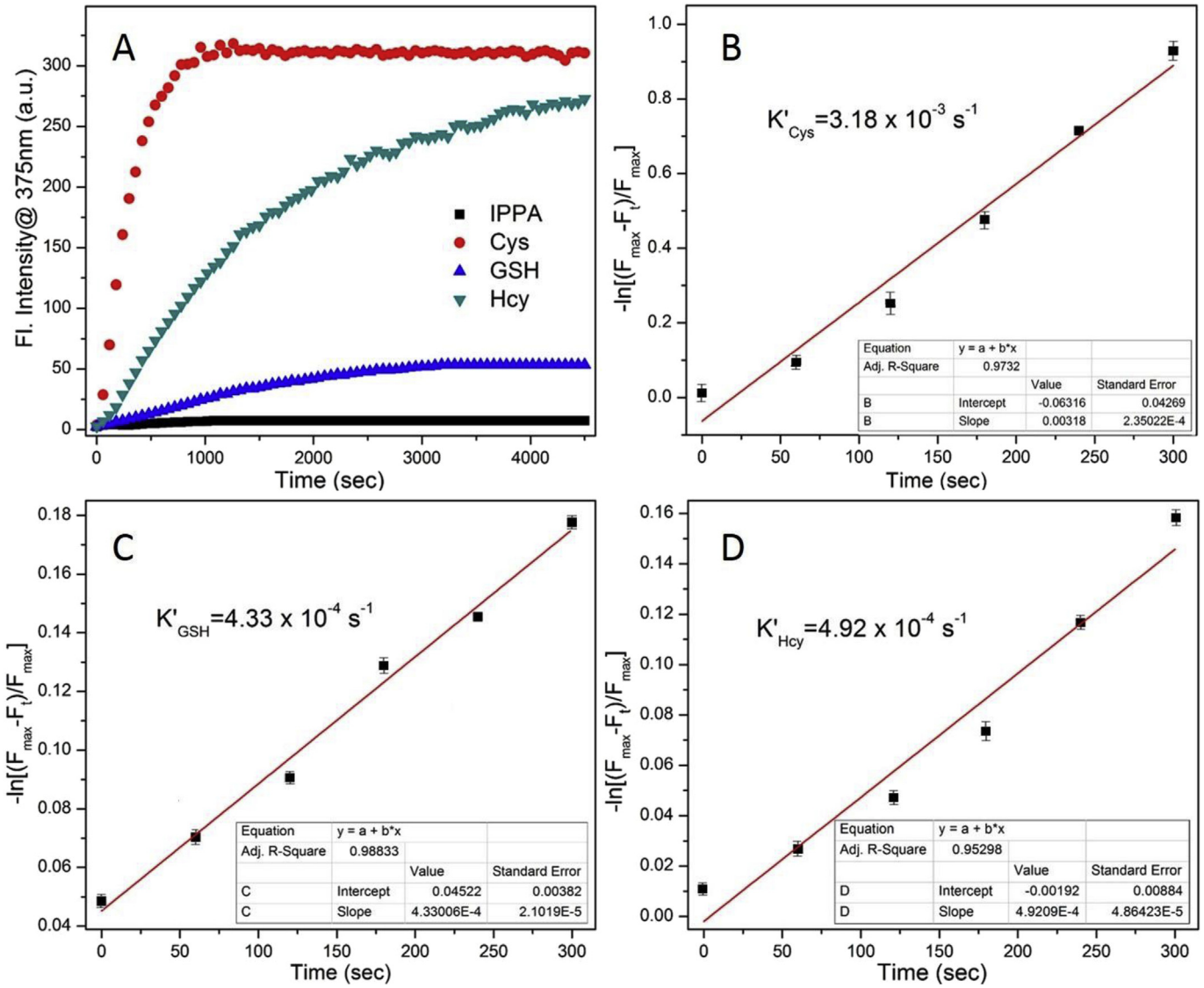

Fig. 1. Time-dependent fluorescence response and pseudo-first-order kinetic plots of **IPPA** (10 μM) at 375 nm with and without biothiols (200 μM) in DMSO-HEPES buffer solution (pH 7.4, 8:2, v/v, λ_{ex} = 330 nm, slit: 10 nm). Data are the mean ± SE (bars) (n = 3).

3.2. Optimization of determination condition

In the present work, the response time of the probe **IPPA** to biothiols was studied. Cys, Hcy and GSH were separately added to DMSO-HEPES buffer solutions (pH 7.4, 8:2, v/v) containing **IPPA**. The response time was measured based on the fluorescence emission spectrum (Fig. 1A). The results showed that the probe **IPPA** can react with Cys rapidly and that the fluorescence intensity was stable in approximately 12 min. However, the reaction time of Hcy and GSH with **IPPA** were significantly (14-fold) lower than that of Cys, and their reaction time was approximately 50 min.

The pH value is another important factor that can influence the reaction. We investigated the fluorescence intensity of the reaction between **IPPA** and three biothiols in the pH range of 2–12. The fluorescence intensity of the **IPPA** + Cys solution changes continuously with increasing pH value (Fig. S7). Obviously, in the pH range from 2.0 to 4.0, the fluorescence intensity of **IPPA** + Cys is rapidly enhanced and slowly increases with the increase of pH value (4–7.4). While the pH value is over 7.4, the fluorescence intensity decreases significantly. In addition, the similar fluorescence change can be seen in the presence of Hcy/GSH. Therefore, the physiological pH of 7.4 were used in all experiments.

The effect of DMSO concentration on the reaction of **IPPA** and biothiols was also investigated. The fluorescence intensity of **IPPA**

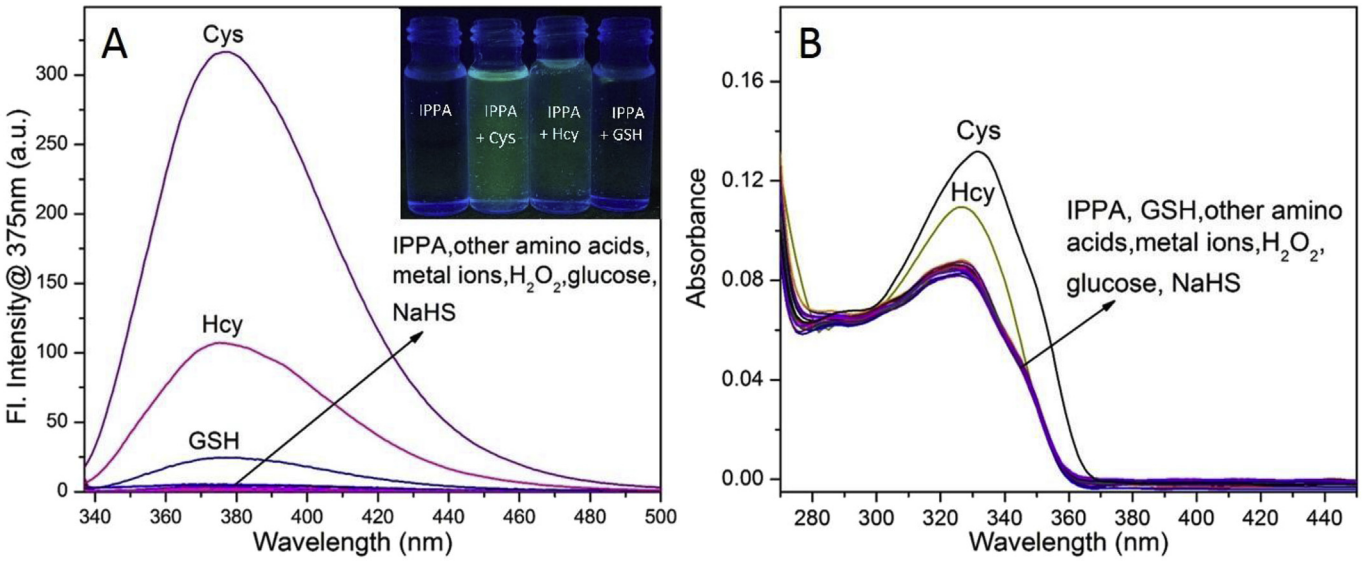

Fig. 2. Fluorescence (A) and UV–Vis spectra (B) of the probe **IPPA** (10 μM) when multiple different analytes (200 μM) were added. The inset is a photograph of **IPPA** solutions with and without biothiols. Data are the mean ± SE (bars) (n = 3).

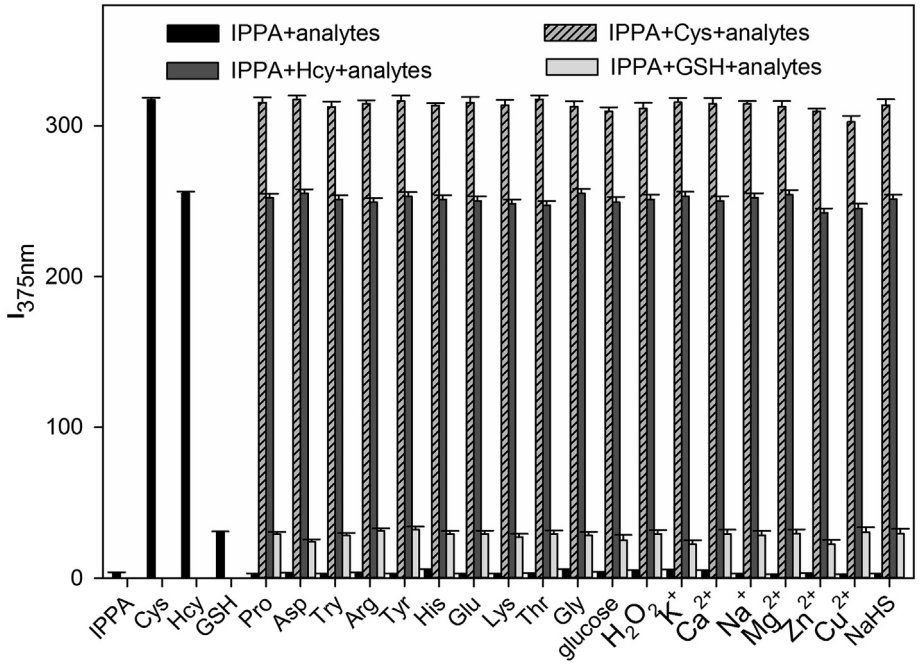

Fig. 3. Fluorescence intensity (I_{375nm}) of **IPPA** (10 μM) without and with biothiols (200 μM) in the presence of various analytes (200 μM) in a DMSO-HEPES buffer solution (pH 7.4, 8:2, v/v, λ_{ex} = 330 nm, slit: 10.0 nm). Data are the mean ± SE (bars) (n = 3).

in the absence and presence of biothiols in solutions with different ratios of DMSO and HEPES is listed in Fig. S8. Ultimately, we chose 8/2 DMSO/HEPES buffer (v/v, pH 7.4) and used it for all experiments.

3.3. Selectivity of ***IPPA***

With the probe in hand, we investigated the response of **IPPA** to various analytes, including thiol-containing amino acids (Cys, Hcy and GSH), other amino acids (Pro, Try, Tyr, Arg, His, Lys, Asp, Thr, Glu, Gly), various ions (K^+, Ca^{2+}, Na^+, Cu^{2+}, Mg^{2+}, Zn^{2+}, Fe^{3+} and HS^-), H_2O_2 and glucose. As shown in Fig. 2B, the UV–Vis spectrum of **IPPA** changes significantly with the addition of Cys/Hcy, with an absorption peak appearing at 330 nm. The absorption spectra of the solution recorded upon titration indicated that the absorption of the peak at 330 nm with the addition of Cys and Hcy (Fig. S10). In Fig. 1A, the probe **IPPA** has almost no fluorescence, but its fluorescence increases in the presence of biothiols. With the addition of Cys and Hcy to the solution of the probe **IPPA** (10 μM), the fluorescence intensity exhibited a 76- and 51-fold enhancement, respectively. However, compared to that of the solution without GSH, the fluorescence intensity of the solution with GSH increased only 14-fold. The addition of other amino acids and various analytes hardly caused any changes in the fluorescent signal (Fig. 2A). In Fig. 2A (inset), under excitation with 365 nm UV light, the color of the **IPPA** solution changed from weak blue to stronger blue-green after adding Cys/Hcy. By contrast, there was no significant change after adding GSH to the probe solution. The results indicate that the probe can specifically recognize Cys/Hcy over GSH. In addition, we calculated the pseudo first-order rate constants of reactions between the probe **IPPA** (10 μM) and the three biothiols. The pseudo-first-order rate constants from Cys, Hcy and GSH are obtained by the linear relationships in Fig. 1 as $K = 3.18 \times 10^{-3}$, 4.33×10^{-4} and $4.92 \times 10^{-4}\ S^{-1}$, respectively. K_{Cys} is approximately 15 times K_{Hcy} and K_{GSH}. Comparison of the pseudo-first-order rate constants reveals that **IPPA** can selectively recognize Cys over Hcy and GSH.

We also investigated the effect of various interfering substances on the recognition of biothiols by **IPPA**, including thiol-containing amino acids (Cys, Hcy and GSH), other amino acids (Pro, Try, Tyr, Arg, His, Lys, Asp, Thr, Glu, Gly), various ions (K^+, Ca^{2+}, Na^+, Cu^{2+}, Mg^{2+}, Zn^{2+}, Fe^{3+} and HS^-), H_2O_2 and glucose. Fig. 3 shows that except for the biothiols, most of analytes do not cause fluorescence

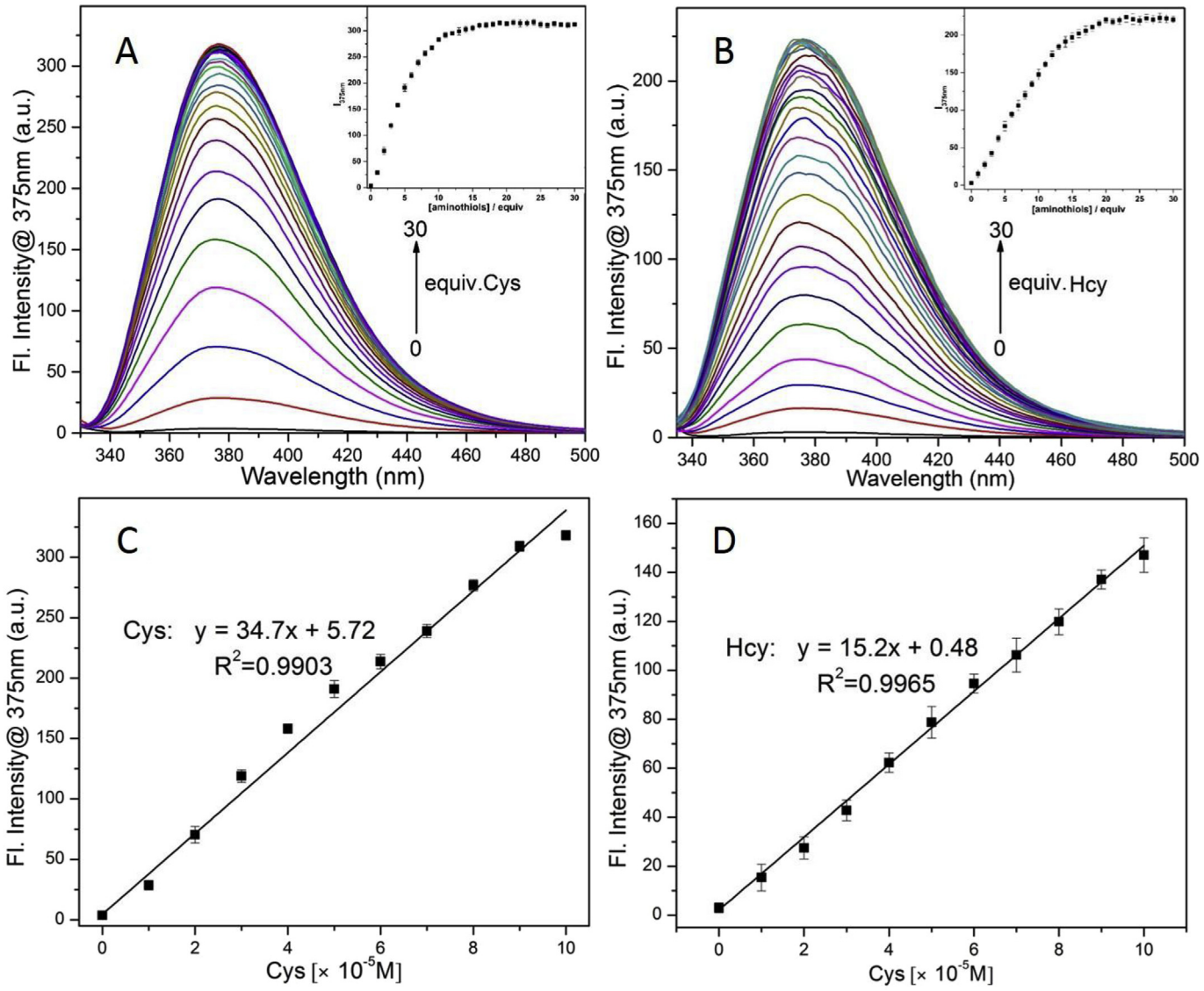

Fig. 4. Fluorescence titration spectra of **IPPA** (10 μM) vs Cys, GSH and Hcy (0–30 equiv.) in a DMSO-HEPES buffer solution (pH 7.4, 8:2, v/v, $\lambda_{ex} = 330$ nm). Plot of fluorescence intensity at 375 nm as a function of biothiol equivalents. Data are the mean ± SE (bars) (n = 3).

enhancement. These results revealed that the probe **IPPA** can selectively detect Cys/Hcy over other analytes.

3.4. Quantification of biothiols

To further study the quantitative response of **IPPA** to the presence of different concentrations of biothiols, fluorescence and UV–Vis titration experiments were performed. In Fig. S9, the maximum absorption wavelength of **IPPA** is approximately 330 nm. The addition of Cys and Hcy results in an increase in the intensity of the absorption peak of **IPPA**. Fig. S9A shows that the addition of Cys causes a slight redshift, while the addition of Hcy has no effect on the maximum absorption wavelength of **IPPA** (Fig. S9B). The fluorescence quantum yield of **IPPA** was calculated as 0.011 and became 0.52/0.21 with the addition of Cys/Hcy, respectively; this strong fluorescence indicates that **IPPA** was converted into another product. The result was consistent with that of the titration experiment. As shown in Fig. 4, **IPPA** exhibits no fluorescence at 375 nm. However, the fluorescence intensity increased as the concentration of biothiols increased, and has a good linear relationship with the biothiol concentration. In the presence of 30 equiv. Cys/Hcy/GSH, the fluorescence intensity of **IPPA** undergoes 76, 51 and 14-fold enhancement, respectively. The limits of detection (LOD) of Cys and Hcy were calculated using the detection limit formula (CDL = 3 Sb/m) to be 0.33 and 0.76 μM, respectively (Fig. S10). Compared to the recently reported probes for the detection of biothiols (Table S2), **IPPA** exhibits low detection limits, low molecular weight and short detection time.

3.5. Mechanism of detection

The mechanism of the reaction between **IPPA** and biothiols was investigated with NMR analysis of the DMSO-d_6 solution of **IPPA** and one of biothiols (mol ratio, **IPPA**: biothiols = 1:1) at ambient temperature. In Fig. 5, the hydrogen atoms on the acrylate group were located at 6.59 ppm (2H) and 6.20 ppm (1H). After adding the biothiols, the hydrogen atoms on the acrylate group disappear, which is accompanied by the appearance of new peaks. The results indicated that biothiols react with **IPPA** at the acrylate group, which causes the acrylate group to fall off **IPPA**.

The reaction mechanism was also investigated via analysis of the products of the reaction between **IPPA** and biothiols by LC-HRMS (Table S1, Figs. S12–13). The results indicate that the biothiol is conjugated with the olefinic double-bond in the probe to form a thioether (calcd [H^+]: **IPPA**-Cys/**IPPA**-Hcy, 386.1169/400.1326; found *m*/*z*: Cys/Hcy, 386.1172/400.1322). **IPPA**-Cys and **IPPA**-Hcy can be further cyclized to release the former fluorophore **HPIP**. However, the thioether produced by GSH is stable and the subsequent cyclization efficiency is low. Therefore, in the **IPPA**-GSH system, minimal fluorescence was generated. The cyclization process of Cys generates a seven-membered ring (calcd [H^+]: 176.0376; found *m*/*z*: 176.0390), while that of Hcy generates an eight-membered ring (calcd [H^+]: 190.0532; found *m*/*z*: 190.0542). Generally, the strain in tension of the eight-membered ring is much higher than that in the seven-membered ring, and the activation entropy of the formation reaction of an eight-membered ring needs more energy (Scheme 2). Thus, the formation rate of the seven-membered ring is much faster than that of the eight-membered ring. As a result, the selectivity of **IPPA** for Cys can be achieved because of the difference in reaction rate.

3.6. The density functional theory (DFT) calculation

To better understand the fluorescence performance of **IPPA**, density functional theory (DFT) calculation was performed using the B3LYP method on the Gaussian 09 program [58–60], and the

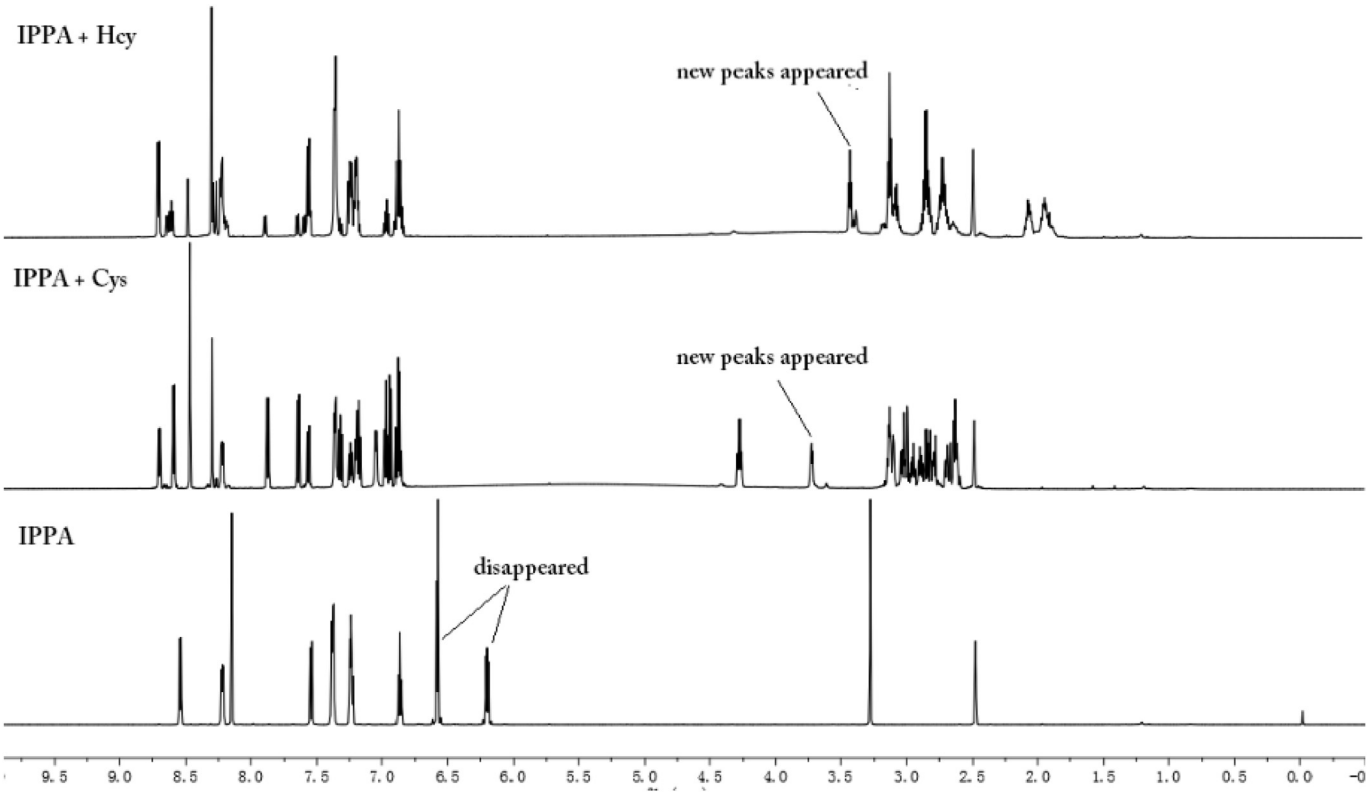

Fig. 5. ^{1}H NMR spectrum of **IPPA** in d_6-DMSO and the resulting spectra after the addition of Cys and Hcy.

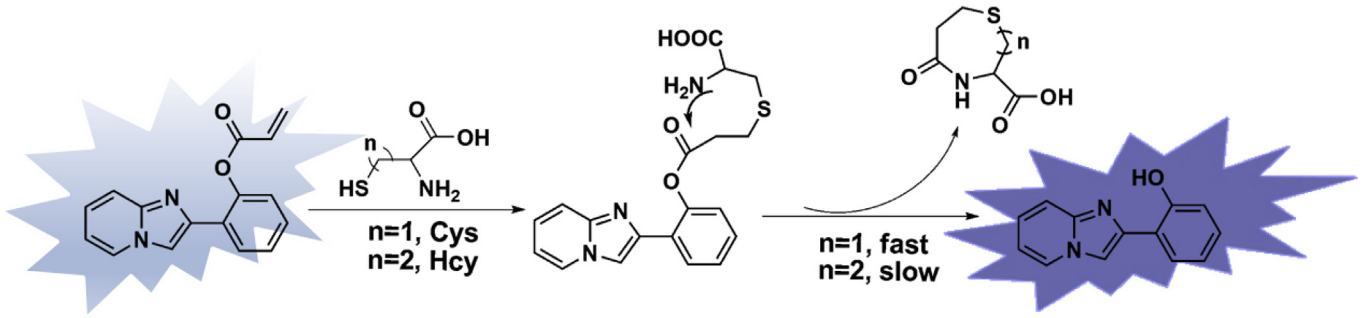

Scheme 2. Proposed mechanism of 2-(imidazo[1,2-a]pyridin-2-yl)phenyl acrylate (**IPPA**) for biothiol sensing.

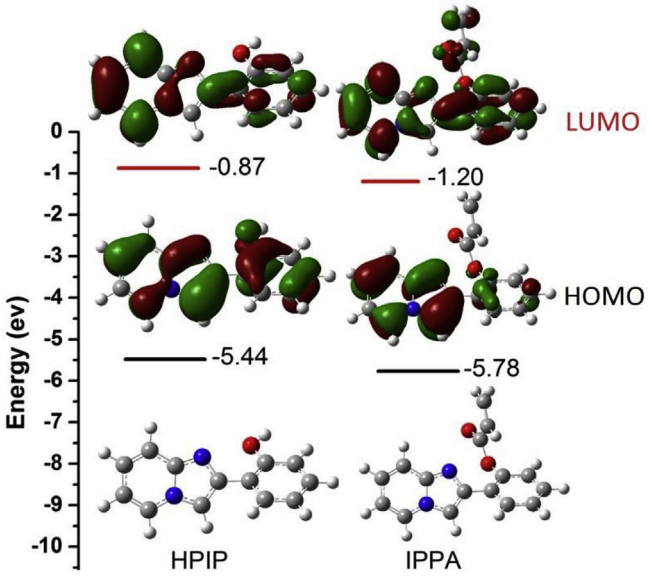

Fig. 6. HOMO and LUMO of **IPPA** and **HPIP**.

spatial distribution and orbital energy of **HPIP** and **IPPA** were optimized (Figs. S13–S14). The highest occupied molecular orbital (HOMO) and the lowest unoccupied molecular orbital (LUMO) of **HPIP** and **IPPA** are shown in Fig. 6. The LUMO is localized almost all over the **IPPA** molecule, while the HOMO is mainly distributed on the imidazo-pyridine moiety. Upon fluorescence excitation, the recognition group blocks the fluorescence emission of **IPPA**, resulting in fluorescence quenching. Notably, when **IPPA** reacts with one biothiol, the acrylate group is attacked due to the Michael addition cyclization reaction, and the product **HPIP** is formed. Moreover, the HOMO of **HPIP** is distributed on the fluorophore, indicating that **IPPA** will show strong fluorescence when reacted with an amino mercaptan. The above theoretical findings are consistent with the experimental results, and confirm the previously proposed mechanism.

3.7. Real application of *IPPA*

To study the application of **IPPA** in actual conditions, the fluorescence response of **IPPA** toward calf serum in an aqueous HEPES buffer (pH 7.4, DMSO content < 0.2%) at ambient temperature was investigated. We performed an experiment with NEM as the block

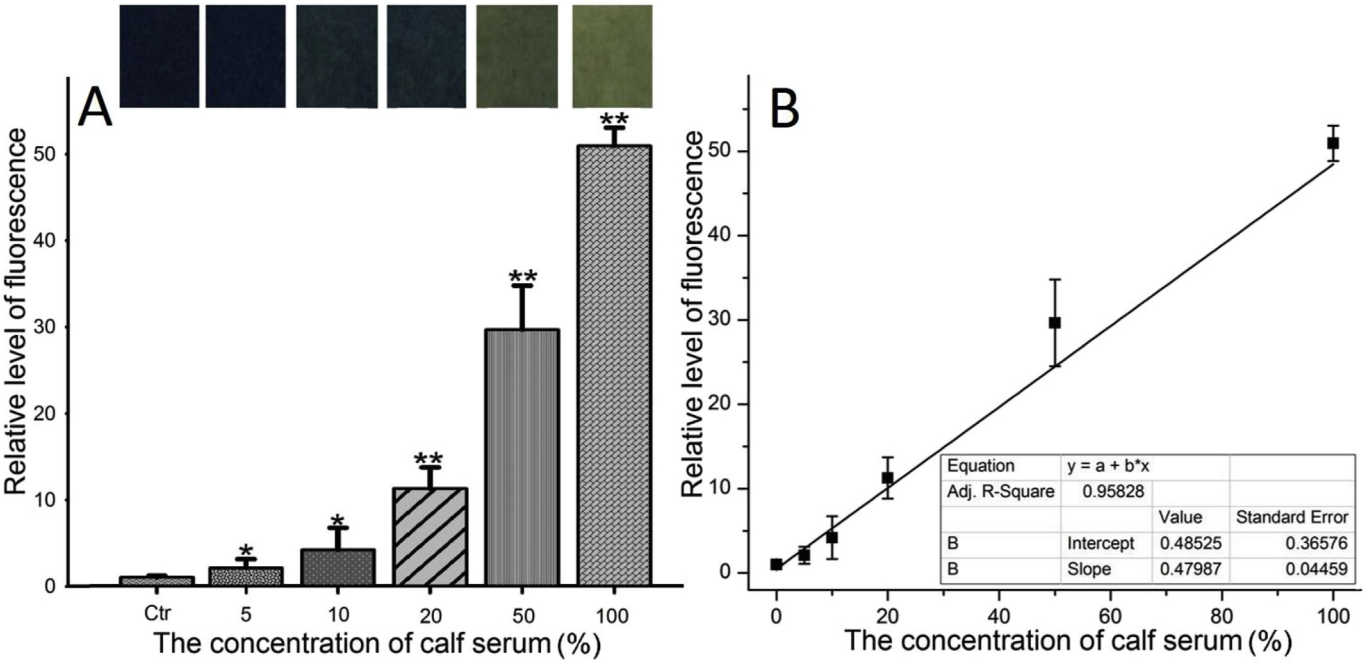

Fig. 7. (A) Relative fluorescence intensity of calf serum with **IPPA** (10 μM) in an aqueous HEPES buffer (pH 7.4, DMSO content < 0.2%), λex = 330 nm; (B) the correlation curve between relative fluorescence intensity and calf serum content. Data are the mean ± SE (bars) (n = 3).

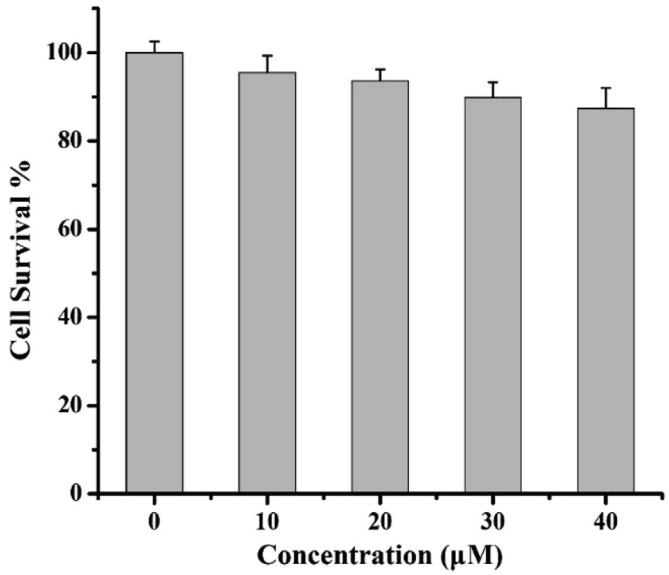

Fig. 8. Cell viability values (%) estimated by a CCK-8 assay versus incubation concentrations of **IPPA**. HepG2 cells were cultured in the presence of 0–40 μM **IPPA**. Data are the mean ± SE (bars) (n = 3).

agent in calf serum to verify that the increase in fluorescence is related to the biothiols content in calf serum. As shown in Fig. S15, there is no obvious fluorescent change in the presence of NEM in calf serum. However, observation of the increasing fluorescence intensity in the absence of NEM indicated this increase can be definitely confirmed to biothiols in calf serum. The fluorescence intensity of **IPPA** increased with the increase of calf serum content (Fig. 7A). It is exciting that the fluorescence intensity has a good linear relationship with calf serum content (R^2, 0.958). Therefore, **IPPA** can determine the content of calf serum with the detection of the biothiols in calf serum.

In addition, a test strip experiment was carried out. First, the test paper was cut into small pieces and immersed in **IPPA** solution. Once the test trip was dry, various analytes (Pro, Asp, Try, Arg, Tyr, His, Glu, Lys, Thr, glucose, K^+, Ca^{2+}, Na^+, Mg^{2+}, Zn^{2+}, Fe^{3+}, Cu^{2+}, H_2O_2, NaHS, Cys, Hcy and GSH) were separately dropped on the test strips. In Fig. S16, the **IPPA**-Cys/**IPPA**-Hcy strips changed from colorless to an intense blue-green fluorescence under excitation with a 365 nm UV lamp, while the change in the color of the **IPPA**-GSH strip was not obvious. The other analyte changes were also negligible. Therefore, **IPPA** test strips can be effectively applied in the detection of Cys/Hcy.

3.8. Study of cytotoxicity and cell imaging

To investigate the effect of **IPPA** on cells, the cytotoxicity was studied by a CCK-8 assay. HepG2 cells were incubated in probe solutions (0, 10, 20, 30 and 40 μM) for 24 h to observe cell survival. As shown in Fig. 8, even when the probe **IPPA** concentration was increased to 40 μM, the survival rate of HepG2 cells was still greater than 85%. The experimental results show that **IPPA** has low toxicity to cells and can be further used for cell imaging research.

Next, we performed live HepG2 cell imaging experiments with **IPPA** under a fluorescence microscope. In Fig. 9, HepG2 cells that were not treated with NEM showed significant fluorescence after incubation with **IPPA** for 20 min, while no fluorescence changes were observed in HepG2 cells treated with NEM. To further investigate the ability of **IPPA** to detect the three biothiols in HepG2 cells, we designed three groups of controlled trials as follows: HepG2 cells were pretreated with NEM (1.0 mM) for 1 h and then incubated with GSH, Hcy or Cys (20 μM) for 20 min. The combined images indicate that **IPPA** has satisfactory cell membrane permeability, which allows it to sensitively detect Cys and Hcy at endogenous levels in HepG2 cells. The results of cell imaging reveal that **IPPA** has potential for bioapplication in detecting intracellular Cys/Hcy.

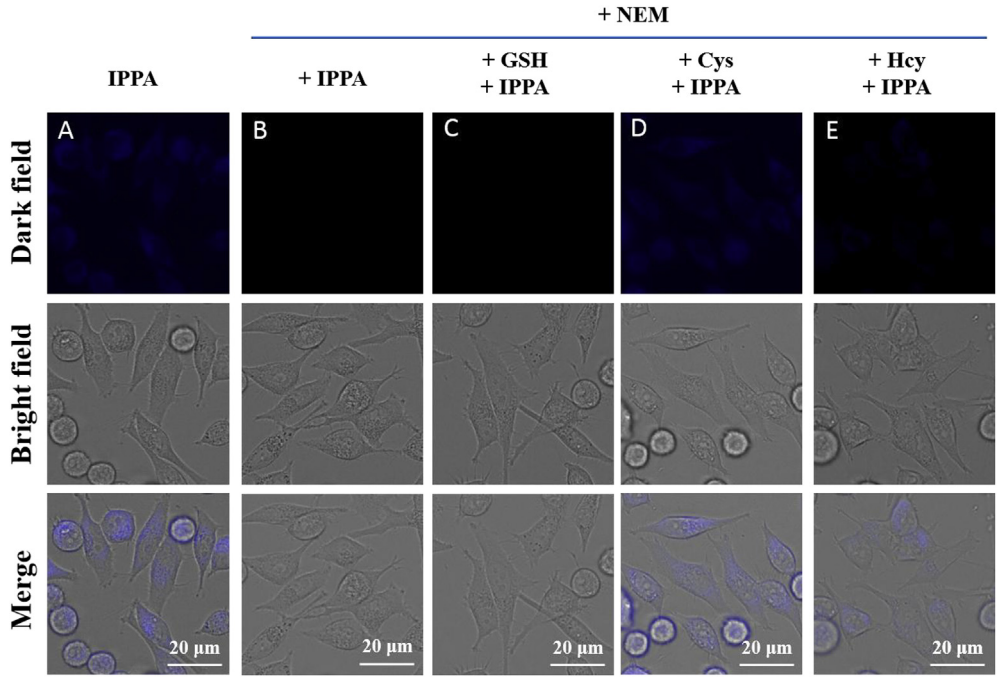

Fig. 9. Fluorescence imaging of Cys/Hcy in living HepG2 cells. From left to right: HepG2 cells incubated with **IPPA** (20 μM) for 20 min (A); HepG2 cells pretreated with NEM (1 mM) for 1 h and then incubated with **IPPA** (20 μM) for 20 min (B); the last three groups of HepG2 cells pretreated with NEM (1.0 mM) for 1 h, then incubated with GSH (C), Cys (D), or Hcy (E) (20 μM) for 20 min, and finally incubated with **IPPA** (20 μM) for 20 min. From top to bottom: Dark field (UV light), Bright field, Merge. Scale bar: 20 μm.

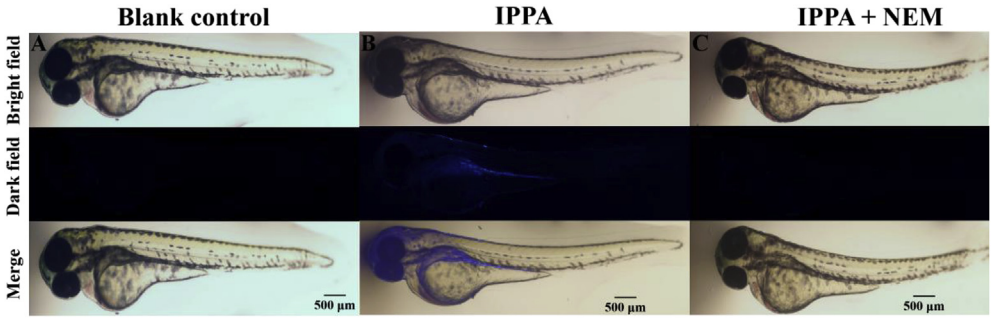

Fig. 10. Fluorescence imaging of zebrafish. From left to right: zebrafish incubated without **IPPA** (20 μM) (A); zebrafish pretreated with **IPPA** (20 μM) for 20 min (B); zebrafish pretreated with NEM (200 μM) for 15 min and then incubated with **IPPA** (20 μM) for 20 min (C). From top to bottom: Bright field, Dark field (UV light), Merge. Scale bar: 500 μm.

3.9. Zebrafish imaging

To further confirm the bioapplication potential of **IPPA**, zebrafish imaging was performed using the probe **IPPA**. As shown in Fig. 10, when the zebrafish were incubated with the probe (20 μM) for 30 min, blue fluorescence was observed in the UV channel. However, when the zebrafish were incubated with NEM (200 μM) for 15 min and then incubated with **IPPA** (20 μM) for 30 min, no fluorescence was observed. NEM also blocks the interaction of **IPPA** and biothiols in the zebrafish. Clearly, the probe **IPPA** can be used to visualize Cys/Hcy in the zebrafish.

4. Conclusions

We designed and synthesized a small-molecule fluorescent probe using an acryloyl group as a recognition group. The probe **IPPA** can selectively and sensitively distinguish Cys from other interferents. In addition, the reaction mechanism was studied by DFT calculation, HRMS and NMR. **IPPA** can also be used to detect biothiols in the test strip and calf serum. Moreover, **IPPA** was successfully applied for imaging in live HepG2 cells and zebrafish. The simple, inexpensive and efficient preparation of **IPPA** showed potential advantages in the detection of Cys in vivo. This study can provide useful information for possibility of further structural optimization for improving the sensing behavior. In addition, red or near-infrared dual-light water-soluble fluorescent probes can be designed to improve in vivo diagnostic applications in rodents or mammalians in our future studies.

Declaration of interests

The authors declare that they have no known competing financial interests or personal relationships that could have appeared to influence the work reported in this paper.

The authors declare the following financial interests/personal relationships which may be considered as potential competing interests.

Acknowledgements

This work was sponsored in part by the Natural Science Foundation of China (No. 31601657 and 21602043), NIEHS R01 ES002710 and Superfund Program P42 ES004699.

Appendix A. Supplementary data

Supplementary data to this article can be found online at https://doi.org/10.1016/j.aca.2019.01.023.

References

[1] D.J. Yu, X.M. Zhang, Y.X. Qi, S.S. Ding, S.M. Cao, A.W. Zhu, G.Y. Shi, Pb^{2+}-modified graphene quantum dots as a fluorescent probe for biological aminothiols mediated by an inner filter effect, Sensor. Actuator. B Chem. 235 (2016) 394–400.
[2] P. Anees, J. Joseph, S. Sreejith, N.V. Menon, Y.J. Kang, S.W.K. Yu, A. Ajayaghosh, Y.L. Zhao, Real time monitoring of aminothiol level in blood using a near-infrared dye assisted deep tissue fluorescence and photoacoustic bimodal imaging, Chem. Sci. 7 (2016) 4110–4116.
[3] Y. Ma, S.J. Liu, H.R. Yang, Y.Q. Wu, H.B. Sun, J.X. Wang, Q. Zhao, F.Y. Li, W. Huang, A water-soluble phosphorescent polymer for time-resolved assay and bioimaging of cysteine/homocysteine, J. Mater. Chem. B 1 (2013) 319–329.
[4] C.C. Huang, W.L. Tseng, Role of fluorosurfactant-modified gold nanoparticles in selective detection of homocysteine thiolactone: remover and sensor, Anal. Chem. 80 (2008) 6345–6350.
[5] M.S. Elgawish, N. Kishikawa, N. Kuroda, Quinones as novel chemiluminescent probes for the sensitive and selective determination of biothiols in biological fluids, Analyst 140 (2015) 8148–8156.
[6] Y. Zhao, Z.J. Hai, H.Y. Wang, L.H. Su, G.L. Liang, Legumain-specific near-infrared fluorescence “turn on” for tumor-targeted imaging, Anal. Chem. 90 (2018) 8732–8735.
[7] S.J. Li, Y.J. Fu, C.Y. Li, Y.F. Li, L.H. Yi, O.Y. Juan, A near-infrared fluorescent probe based on BODIPY derivative with high quantum yield for selective detection of exogenous and endogenous cysteine in biological samples, Anal. Chim. Acta 994 (2017) 73–81.
[8] Q.H. Hu, C.M. Yu, X.T. Xia, F. Zeng, S.Z. Wu, A fluorescent probe for simultaneous discrimination of GSH and Cys/Hcy in human serum samples via distinctly-separated emissions with independent excitations, Biosens. Bioelectron. 81 (2016) 341–348.
[9] X.D. Guo, X. Zhang, S.Q. Wang, S.Y. Li, R. Hu, Y. Li, G.Q. Yang, Sensing for intracellular thiols by water-insoluble two-photon fluorescent probe incorporating nanogel, Anal. Chim. Acta 869 (2015) 81–88.
[10] Q. Wang, X.D. Wei, C.J. Li, Y.S. Xie, A novel p-aminophenylthio- and cyano-substituted BODIPY as a fluorescence turn-on probe for distinguishing cysteine and homocysteine from glutathione, Dyes Pigments 148 (2018) 212–218.
[11] Y. Tian, B.C. Zhu, W. Yang, J. Jing, X.L. Zhang, A fluorescent probe for differentiating Cys, Hcy and GSH via a stepwise interaction, Sensor. Actuator. B Chem. 262 (2018) 345–349.
[12] S.V. Mulay, Y. Kim, M. Choi, D.Y. Lee, J. Choi, Y. Lee, S. Jon, D.G. Churchill, Enhanced doubly activated dual emission fluorescent probes for selective imaging of glutathione or cysteine in living systems, Anal. Chem. 90 (2018) 2648–2654.
[13] Y. Gao, Y. Li, X. Zou, H. Huang, X.G. Su, Highly sensitive and selective detection of biothiols using graphene oxide-based “molecular beacon”-like fluorescent probe, Anal. Chim. Acta 731 (2012) 68–74.
[14] A.C. Sedgwick, H.H. Han, J.E. Gardiner, S.D. Bull, X.P. He, T.D. James, The development of a novel and logic based fluorescence probe for the detection of peroxynitrite and GSH, Chem. Sci. 9 (2018) 3672–3676.
[15] A.Q. Ke, A.D. Liu, Y.N. Gao, D.N. Luo, Z.F. Li, Y.Q. Yu, J.Y. Liu, H. Xu, X. Cao, Development of novel affinity reagents for detecting protein tyrosine phosphorylation based on superbinder SH_2 domain in tumor cells, Anal. Chim. Acta 1032 (2018) 138–146.
[16] F.T.C. Moreira, B.A.G. Rodriguez, R.A.F. Dutra, M.G.F. Sales, Redox probe-free readings of a beta-amyloid-42 plastic antibody sensory material assembled on copper@carbon nanotubes, Sensor. Actuator. B Chem. 264 (2018) 1–9.
[17] B. Li, Y.L. Yu, F.Q. Xiang, S.Y. Zhang, Z.W. Gu, Latent naphthalimide bearing water-soluble nanoprobes with catechol-Fe(III) cores for in vivo fluorescence imaging of intracellular thiols, ACS Appl. Mater. Interfaces 10 (2018) 16282–16290.
[18] S.P. Kwon, S. Jeon, S.H. Lee, H.Y. Yoon, J.H. Ryu, D. Choi, J.Y. Kim, J. Kim, J.H. Park, D.E. Kim, I.C. Kwon, K. Kim, C.H. Ahn, Thrombin-activatable

fluorescent peptide incorporated gold nanoparticles for dual optical/computed tomography thrombus imaging, Biomaterials 150 (2018) 125–136.
[19] H. Wang, S.C. Liang, Z.M. Zhang, H.S. Zhang, 3-iodoacetylaminobenzanthrone as a fluorescent derivatizing reagent for thiols in high-performance liquid chromatography, Anal. Chim. Acta 512 (2004) 281–286.
[20] S. Ruseva, A. Vasileva, D. Aleksandrova, V. Lozanov, V. Mitev, Liquid chromatography orbitrap mass spectrometry method for analysis of homocysteine and related aminothiols in cereal products, Food Anal. Method 7 (2014) 865–871.
[21] S.S. Li, Q.Y. Guan, M.M. Zheng, Y.Q. Wang, D.J. Ye, B. Kang, J.J. Xu, H.Y. Chen, Simultaneous quantification of multiple endogenous biothiols in single living cells by plasmonic Raman probes, Chem. Sci. 8 (2017) 7582–7587.
[22] R.S. Na, M.Q. Zhu, S.S. Fan, Z. Wang, X.W. Wu, J. Tang, J. Liu, Y. Wang, R.M. Hua, A simple and effective ratiometric fluorescent probe for the selective detection of cysteine and homocysteine in aqueous media, Molecules 21 (2016) 1023–1031.
[23] Y. Wang, M.Q. Zhu, E.K. Jiang, R.M. Hua, R.S. Na, Q.X. Li, A simple and rapid turn on ESIPT fluorescent probe for colorimetric and ratiometric detection of biothiols in living cells, Sci. Rep. UK 7 (2017) 4377.
[24] Y. Wang, L.J. Wang, E.K. Jiang, M.Q. Zhu, Z. Wang, S.S. Fan, Q. Gao, S.Z. Liu, Q.X. Li, R.M. Hua, A colorimetric and ratiometric dual-site fluorescent probe with 2,4-dinitrobenzenesulfonyl and aldehyde groups for imaging of aminothiols in living cells and zebrafish, Dyes Pigments 156 (2018) 338–347.
[25] Q. Wang, F.T. Ma, W.Q. Tang, S.L. Zhao, C.J. Li, Y.S. Xie, A novel nitroethylene-based porphyrin as a NIR fluorescence turn-on probe for biothiols based on the Michael addition reaction, Dyes Pigments 148 (2018) 437–443.
[26] J. Zhou, L.C. Meng, W.R. Ye, Q.L. Wang, S.Z. Geng, C. Sun, A sensitive detection assay based on signal amplification technology for Alzheimer's disease's early biomarker in exosome, Anal. Chim. Acta 1022 (2018) 124–130.
[27] Q.C. Mo, F. Liu, J. Gao, M.P. Zhao, N. Shao, Fluorescent sensing of ascorbic acid based on iodine induced oxidative etching and aggregation of lysozyme-templated silver nanoclusters, Anal. Chim. Acta 1003 (2018) 49–55.
[28] W.Y. Li, J.C. Zhu, G.C. Xie, Y.K. Ren, Y.Q. Zheng, Ratiometric system based on graphene quantum dots and Eu^{3+} for selective detection of tetracyclines, Anal. Chim. Acta 1022 (2018) 131–137.
[29] J.H. Lee, C.S. Lim, Y.S. Tian, J.H. Han, B.R. Cho, A two-photon fluorescent probe for thiols in live cells and tissues, J. Am. Chem. Soc. 133 (2011), 7234-7234.
[30] B. Liu, J.F. Wang, G. Zhang, R.K. Bai, Y. Pang, Flavone-based ESIPT ratiometric chemodosimeter for detection of cysteine in living cells, ACS Appl. Mater. Interfaces 6 (2014) 4402–4407.
[31] W.X. Ren, J. Han, T. Pradhan, J.Y. Lim, J.H. Lee, J. Lee, J.H. Kim, J.S. Kim, A fluorescent probe to detect thiol-containing amino acids in solid tumors, Biomaterials 35 (2014) 4157–4167.
[32] D. Zhang, D.M. Liu, M. Li, Y.Q. Yang, Y. Wang, H.Y. Yin, J.H. Liu, B. Jia, X.J. Wu, A simple pyrene-based fluorescent probe for highly selective detection of formaldehyde and its application in live-cell imaging, Anal. Chim. Acta 1033 (2018) 180–184.
[33] X.F. Yang, Y.X. Guo, R.M. Strongin, A seminaphthofluorescein-based fluorescent chemodosimeter for the highly selective detection of cysteine, Org. Biomol. Chem. 10 (2012) 2739–2741.
[34] H.Y. Zhang, W.Y. Feng, G.Q. Feng, A simple and readily available fluorescent turn-on probe for cysteine detection and bioimaging in living cells, Dyes Pigments 139 (2017) 73–78.
[35] W.L. Fan, X.M. Huang, X.M. Shi, Z. Wang, Z.L. Lu, C.H. Fan, Q.B. Bo, A simple fluorescent probe for sensing cysteine over homocysteine and glutathione based on PET, Spectrochim. Acta A 173 (2017) 918–923.
[36] H.R. Lu, H.T. Zhang, J. Chen, J.C. Zhang, R.C. Liu, H.Y. Sun, Y.L. Zhao, Z.F. Chai, Y. Hu, A thiol fluorescent probe reveals the intricate modulation of cysteine's reactivity by Cu(II), Talanta 146 (2016) 477–482.
[37] L.L. Xia, Y. Zhao, J.X. Huang, Y.Q. Gu, P. Wang, A fluorescent turn-on probe for highly selective detection of cysteine and its bioimaging applications in living cells and tissues, Sensor. Actuator. B Chem. 270 (2018) 312–317.
[38] F.Y. Wang, Y.Y. Zhu, J. Xu, Z.A. Xu, G.Y. Cheng, W. Zhang, Highly selective and ratiometric fluorescent nanoprobe for the detection of cysteine and its application in test strips, Anal. Bioanal. Chem. 410 (2018) 4875–4884.
[39] C.M. Han, H.R. Yang, M. Chen, Q.Q. Su, W. Feng, F.Y. Li, Mitochondria-targeted near-infrared fluorescent off-on probe for selective detection of cysteine in living cells and in vivo, ACS Appl. Mater. Interfaces 7 (2015) 27968–27975.
[40] H.J. Tong, J.H. Zhao, X.M. Li, Y.J. Zhang, S.N. Ma, K.Y. Lou, W. Wang, Orchestration of dual cyclization processes and dual quenching mechanisms for enhanced selectivity and drastic fluorescence turn-on detection of cysteine, Chem. Commun. 53 (2017) 3583–3586.
[41] Y.F. Huang, H.T. Chang, Nile red-adsorbed gold nanoparticle matrixes for determining aminothiols through surface-assisted laser desorption/ionization mass spectrometry, Anal. Chem. 78 (2006) 1485–1493.
[42] Y.J. Lai, W.L. Tseng, Gold nanoparticle extraction followed by o-phthaldialdehyde derivatization for fluorescence sensing of different forms of homocysteine in plasma, Talanta 91 (2012) 103–109.
[43] J.T. Hou, J. Yang, K. Li, K.K. Yu, X.Q. Yu, A colorimetric and red emissive fluorescent probe for cysteine and its application in bioimaging, Sensor. Actuator. B Chem. 214 (2015) 92–100.
[44] Y. Liu, J. Nie, J. Niu, W.S. Wang, W.Y. Lin, An AIE plus ESIPT ratiometric fluorescent probe for monitoring sulfur dioxide with distinct ratiometric fluorescence signals in mammalian cells, mouse embryonic fibroblast and zebrafish, J. Mater. Chem. B 6 (2018) 1973–1983.
[45] X.J. Liu, A.S. Zheng, D.R. Luan, X.T. Wang, F.P. Kong, L.L. Tong, K.H. Xu, B. Tang, High-quantum-yield mitochondria-targeting near-infrared fluorescent probe for imaging native hypobromous acid in living cells and in vivo, Anal. Chem. 89 (2017) 1787–1792.
[46] B. Tang, L.J. Cui, K.H. Xu, L.L. Tong, G.W. Yang, L.G. An, A sensitive and selective near-infrared fluorescent probe for mercuric ions and its biological imaging applications, Chembiochem 9 (2008) 1159–1164.
[47] A.J. Stasyuk, M. Banasiewicz, M.K. Cyranski, D.T. Gryko, Imidazo[1,2-a]pyridines susceptible to excited state intramolecular proton transfer: one-pot synthesis via an ortoleva-king reaction, J. Org. Chem. 77 (2012) 5552–5558.
[48] H.Y. Wang, Q.J. Lu, M.X. Li, H. Li, Y.L. Liu, H.T. Li, Y.Y. Zhang, S.Z. Yao, Electrochemically prepared oxygen and sulfur co-doped graphitic carbon nitride quantum dots for fluorescence determination of copper and silver ions and biothiols, Anal. Chim. Acta 1027 (2018) 121–129.
[49] H. Kaur, P. Raj, H. Sharma, M. Verma, N. Singh, N. Kaur, Highly selective and sensitive fluorescence sensing of nanomolar Zn^{2+} ions in aqueous medium using calix[4]arene passivated carbon quantum dots based on fluorescence enhancement: real-time monitoring and intracellular investigation, Anal. Chim. Acta 1009 (2018) 1–11.
[50] H.S. Zhu, E.K. Wang, J. Li, J. Wang, L-tyrosine methyl ester-stabilized carbon dots as fluorescent probes for the assays of biothiols, Anal. Chim. Acta 1006 (2018) 83–89.
[51] Y.X. Zhou, X.L. Zhang, B. Ren, B. Wu, Z.C. Pei, H. Dong, S-Acetyl migration in synthesis of sulfur-containing glycosides, Tetrahedron 70 (2014) 5385–5390.
[52] A. Weichsel, J.R. Gasdaska, G. Powis, W.R. Montfort, Crystal structures of reduced, oxidized, and mutated human thioredoxins: evidence for a regulatory homodimer, Structure 4 (1996) 735–751.
[53] J.W. Winslow, The reaction of sulfhydryl-groups of sodium and potassium ion-activated adenosine-triphosphatase with N-Ethylmaleimide - the relationship between ligand-dependent alterations of nucleophilicity and enzymatic conformational states, J. Biol. Chem. 256 (1981) 9522–9531.
[54] Z.Y. Chen, Q. Sun, Y.H. Yao, X.X. Fan, W.B. Zhang, J.H. Qian, Highly sensitive detection of cysteine over glutathione and homo-cysteine: new insight into the Michael addition of mercapto group to maleimide, Biosens. Bioelectron. 91 (2017) 553–559.
[55] D. Kand, A.M. Kalle, S.J. Varma, P. Talukdar, A chromenoquinoline-based fluorescent off-on thiol probe for bioimaging, Chem. Commun. 48 (2012) 2722–2724.
[56] V.S. Lin, W. Chen, M. Xian, C.J. Chang, Chemical probes for molecular imaging and detection of hydrogen sulfide and reactive sulfur species in biological systems, Chem. Soc. Rev. 44 (2015) 4596–4618.
[57] Q. Huang, X.F. Yang, H. Li, A ratiometric fluorescent probe for hydrogen sulfide based on an excited-state intramolecular proton transfer mechanism, Dyes Pigments 99 (2013) 871–877.
[58] X.S. Zhang, D.R. Cheng, J.Q. Shi, L. Qin, T.T. Wang, B.X. Fang, QSPR modeling of the logK(ow) and logK(oc) of polymethoxylated, polyhydroxylated diphenyl ethers and methoxylated-, hydroxylated-polychlorinated diphenyl ethers, J. Hazard Mater. 353 (2018) 542–551.
[59] M. Iwamoto, M. Akiyama, K. Aihara, T. Deguchi, Ammonia synthesis on wool-like Au, Pt, Pd, Ag, or Cu electrode catalysts in nonthermal atmospheric-pressure plasma of N-2 and H-2, ACS Catal. 7 (2017) 6924–6929.
[60] P.H. Willoughby, M.J. Jansma, T.R. Hoye, A guide to small-molecule structure assignment through computation of (H-1 and C-13) NMR chemical shifts, Nat. Protoc. 9 (2014) 643–660.